THE ELECTROCHEMISTRY OF SOME PRIMARY CELLS INCORPORATING ZINC ELECTRODES

S. A. G. R. KARUNATHILAKA, N. A. HAMPSON and R. LEEK

University of Technology, Loughborough, Leicestershire, LE11 3TU (U.K.)

T. J. SINCLAIR

Procurement Executive, Ministry of Defence, Royal Armament Research and Development Establishment, Sevenoaks, Kent (U.K.)

Summary

The different electrochemistries of the three main commercial primary cells, the Leclanché cell, the alkaline zinc–mercury oxide cell, and the alkaline zinc–manganese dioxide cell, have been investigated using an automatic impedance measurement technique. The impedance responses over an extended frequency range have been matched to proposed models using a powerful computer technique which is capable of breaking down the experimental data into the individual kinetic process corresponding to each electrode mechanism. The results show how interpretations of the impedance data can be made which enable critical limitations within each system to be recognised. A rather surprising result is the lack of porous characteristics, which are obscured in some situations using electrodes fabricated from amalgamated powders.

Introduction

Zinc is the negative electrode (anode) in a number of primary cells, of which the most important are the Leclanché cell, the alkaline zinc–manganese dioxide cell and the alkaline zinc–mercury oxide cell. In the Leclanché cell the zinc operates in acidic environments while in the latter two cells the zinc is in a finely divided porous form and discharges in alkaline conditions.

These three cells form the majority of the commercial primary cells and underline the importance of zinc as a storage cell electrode. Zinc is used in solid (sheet) form in acid solution but, mainly due to the effect of the hydrogen evolution reaction, it is used as a porous electrode in alkaline media. The hydrogen evolution reaction causes very high open-circuit losses with the porous zinc electrode and it has become the practice to incorporate mercury in the negative systems in order to poison the hydrogen reaction by making use of the high potential for hydrogen evolution on mercury.

0378-7753/83/0000-0000/$03.00

The most searching technique for the investigation of electrochemical reactions is the impedance technique. In this method, originally introduced by Randles [1] and Ershler [2], a small sinusoidal potential is applied to an electrode and the resulting current flow is analysed to obtain the impedance of the system. Originally null methods were the ones usually employed [3], but it is becoming customary to employ frequency response analysers [4]. The modern version of these instruments applies a small sinusoidal perturbation to the electrode system and analyses the resulting current to give the impedance. The instruments can be programmed to estimate the impedances at a series of values over a range of frequencies since it is from the change of impedance with frequency that the kinetic constants of the electrochemical reactions are obtained.

An example of the technique is given in Fig. 1, which records the resistive (R) and capacitive ($1/\omega C$) components of a single electrode impedance. It has become customary [5] to plot each component against the other using frequency as the parameter. At high frequency a charge transfer reaction, *e.g.*:

$$Zn^{2+} + 2e \rightleftharpoons Zn \qquad (1)$$

would appear as a single semicircle. At a lower frequency, diffusion in solution appears as a straight line at 45 °C to the real (R) axis. For a reaction in which zinc undergoes both diffusion in solution and charge transfer we obtain the curve of Fig. 1 over the whole frequency range, which usually extends from about 10 kHz down to 0.001 Hz. For a cell with two electrodes the impedance loci (called Sluyters plots) become complicated. The effects of two charge transfer reactions and two diffusion processes are included, together with the effects of double layer capacitances for each electrode. The latter effect determines the value of the frequency at the top of the high frequency semicircle. We would expect two semicircles

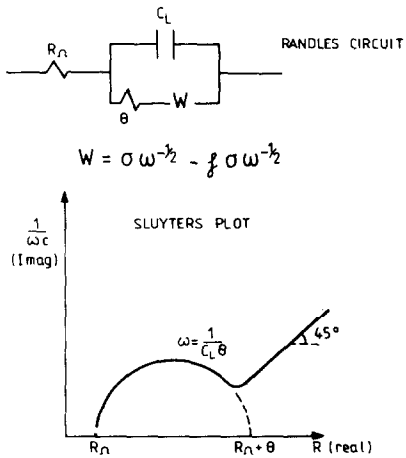

Fig. 1. Simple charge transfer and diffusion.

to be indicative of a cell of two electrodes and this is what we obtain provided that the double layer capacitances differ sufficiently [6].

Figure 2 (a) and (b) shows how two Randles circuits behave when the relative magnitudes change from identically equal to a 5 to 1 ratio for the charge transfer resistance and a 20 to 1 ratio for the double layer capacitances; the single semicircle in Fig. 2(a) for identical components becomes two, well-defined semicircles for the asymmetric case (Fig. 2(b)).

Combinations of this kind are used when we carry out electrochemical investigations on commercial cells. In general, we cannot get into the cell to introduce a third reference electrode and the cell behaviour has to be deduced from the complex picture. In this paper we present the impedance behaviour of the three major commercial primary cells. All use zinc negative electrodes (anodes) in some form; a comparison of the behaviours with the resulting interpretations shows the wide range of behaviour obtained with this electrode metal.

Results and discussion

Figure 3 shows the impedance spectrum of a newly-assembled Leclanché cell. This semicircle at high frequency is elongated and the simple Randles picture will not satisfactorily explain the behaviour. From an estimate of the double layer capacitance of the electrode responsible for the distorted semicircle from the summit of this semicircle, we conclude that it arises from the zinc. As the manganese dioxide is in the form of a highly-dispersed powder (which would have a very low impedance) we can ascribe the distortion of the semicircle to the carbon/manganese dioxide

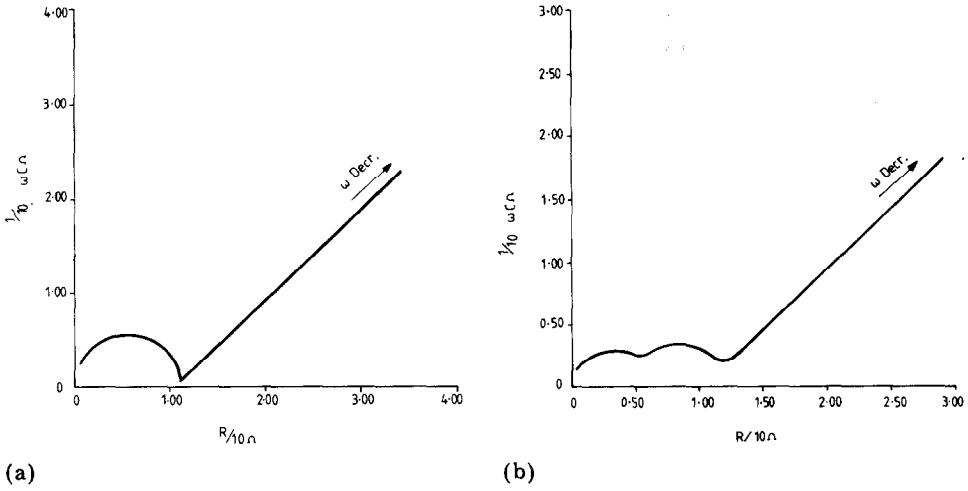

Fig. 2. Two Randles circuits in series. (a) Identical components C_L = 1157 μF, θ = 0.055 Ω, θ = 0.0567 Ω $s^{1/2}$; (b) $C_L{}^1$ = 20 C_L; θ^1 = 0.

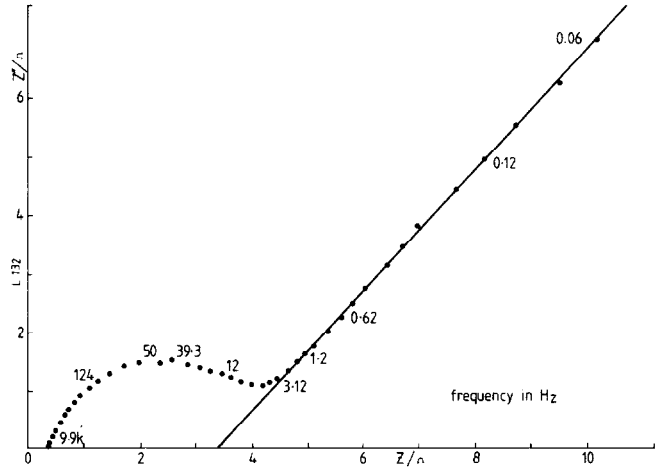

Fig. 3. Impedance loci for newly assembled Leclanché cell (Ever Ready SP11).

interface. This is a parallel combination of a resistance and a capacitance and the whole cell analogue should be as shown in Fig. 4. Calculations using a computer showed that, although the high frequency response was excellent, at low frequency there was still a discrepancy. This was due to surface effects and we modified the working impedance to:

$$W = \sigma_R \omega^{-1/2} - j\sigma_C \omega^{-1/2} \tag{2}$$

where the inequality of σ_R and σ_C may reflect the deviation of the electrode from a perfectly smooth surface. The results of this further refinement are shown in Fig. 5. The fit is good, and was confirmed in the more searching Randles plot in which the impedance components are plotted against $\omega^{-1/2}$. This plot, Fig. 6, shows an excellent correspondence of experimental and calculated data points and the model appears to be entirely adequate.

In Table 1 we compare the kinetic parameters obtained from matching the experimental data for two newly-assembled Leclanché cells with the model shown in Fig. 3. Estimates of the constants obtained from the real (R) and from the imaginary ($1/\omega C$) parts of the electrode impedances which give rise, respectively, to two equations (the R equation and the C equation)

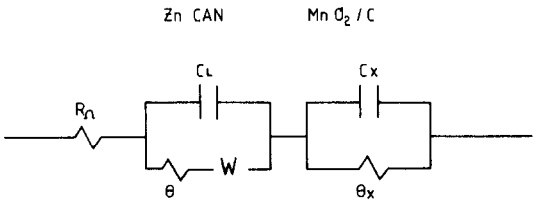

Fig. 4. Cell analogue for the cell of Fig. 3.

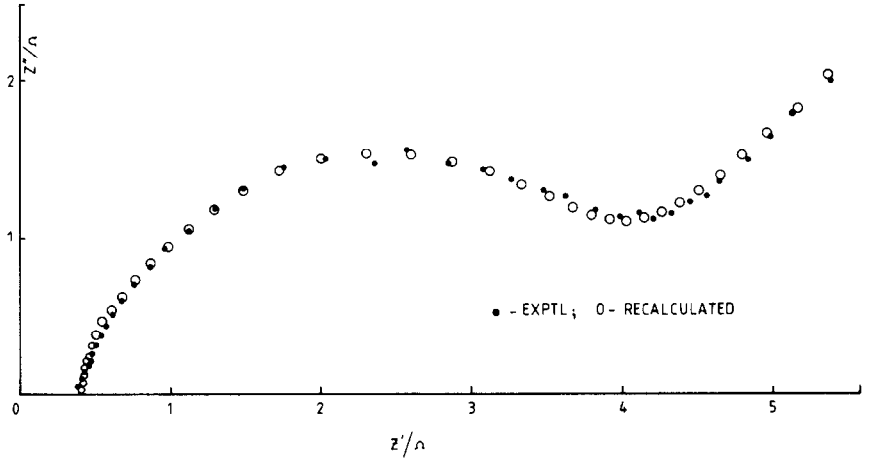

Fig. 5. Data match of Fig. 3 using the analogue of Fig. 4 with a correction for surface roughness.

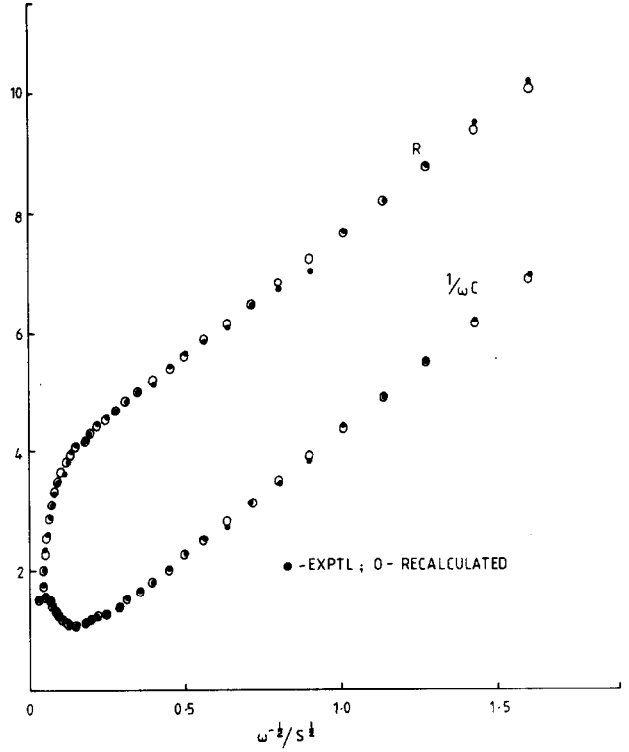

Fig. 6. Randles plot (R and $1/\omega C$ plotted against $\omega^{-1/2}$) corresponding to Fig. 5.

TABLE 1

Salient data for typical Leclanché cells. Type SP11

Model	R_e (Ω)	θ (Ω)	C_L (μF)	θ_x (Ω)	C_x (μF)	σ ($\Omega\ s^{-1/2}$)	σ_R ($\Omega\ s^{-1/2}$)	σ_c ($\Omega\ s^{-1/2}$)
$\sigma_R = \sigma_c$; R eqn.	0.421(19)	2.66(9)	1104(80)	0.56(9)	911(111)	4.09(3)		
$1/\omega C$ eqn.		2.69(5)	1091(42)	0.53(5)	909(79)	4.32(1)		
Cell 1								
$\sigma_R \neq \sigma_c$; R eqn.	0.421(19)	2.68(9)	1087(77)	0.55(9)	911(114)		4.085(30)	
$1/\omega C$ eqn.		2.69(5)	1109(44)	0.55(5)	910(75)			4.328(9)
Cell 2								
$\sigma_R \neq \sigma_c$; R eqn.	0.316(9)	2.52(7)	1720(100)	0.75(8)	1302(66)		3.33(2)	
$1/\omega C$ eqn.		2.42(10)	1975(142)	0.89(11)	1273(112)			3.79(2)

R_t = 84.2(28) Ω cm^2.
CDL = 34.6(25) μF/cm^2.
Approx. area of the zinc can = 31 cm^2.

are tabulated. In principle, the constants can be calculated from either of these equations. From the magnitudes of these constants we have confirmed that it was the zinc can which controlled the cell behaviour. Experiments with individual cell components have also been completed to check that this is so. The inequality of σ_R and σ_C may be due to a number of surface effects; surface roughness would cause $\sigma_C < \sigma_R$, and a measure of the porosity is $\gamma = \sigma_C/\sigma_R$, which is unity for a plane surface and 0.5 for a semi-infinite porous structure. In our case, the higher value of σ_C is to be interpreted as being due to a film of oxide at the electrode surface.

As the Leclanché cell is discharged, the shape of the high frequency semicircle is unaltered. However, the shape of the low frequency line falls, showing that the anodic attack on the zinc electrode is producing a rough surface. At the half discharged condition, Fig. 7 shows that the dihedral angle at low frequency is 22.5° instead of 45° for the plane electrode. This corresponds well to the semi-infinite pore structure, but, a further concomitant of this is that the high frequency semicircle should leave the real axis at 45°, which it does not. We can interpret this as the presence of a limited number of deep pits in the electrode. At high frequencies the major part of the current goes into the flat surface and the behaviour is that of a plane electrode, whilst at low frequencies the penetration depth is considerable and the electrode appears porous since the majority of the current goes into this structure. We have confirmed this conclusion by a physical examination of the zinc from partially discharged cells; the cans were found to be extensively pitted. At higher discharge states, the high frequency semicircles increase in diameter, corresponding to an increase in charge-transfer resistance and a reduction in exchange current density as the active materials

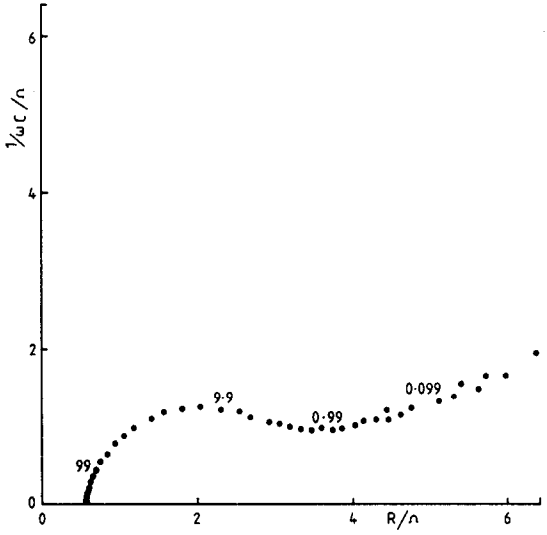

Fig. 7. Impedance loci for Leclanché cell after 50% of the capacity has been removed at the 70 h rate (25 mA for an SP11 cell).

at the electrode become less available. This is shown in Fig. 8 where a relatively large, well-defined semicircle spans the experimental range.

The cells with zinc electrodes in alkali utilise the zinc in a porous form. This powder is prepared by proprietary methods and contains a certain amount of mercury, usually about 5%. The reason for this is that the hydrogen evolution reaction can intrude quite significantly, and incorporation of mercury at this level suppresses the parasitic reaction. Cells are sometimes assembled by forming compacted discs: at other times the zinc amalgam is added in the form of a stiff paste but there appears to be no satisfactory method of including a reference electrode within any of the cell assemblies. Thus, the electrochemistry has to be investigated by considering the cells as two-terminal devices and deducing the electrochemistry from the impedance and a knowledge of the chemistry of the electrode and solution processes.

For the alkaline zinc–mercury oxide cell, the impedance spectrum for the newly assembled cell is shown in Fig. 9. Here we observe the characteristic semicircle at high frequency followed by a lower frequency line, at about 38° to the real axis, which returns to the real axis as the frequency is reduced to very low values. Discharging the cell resulted in relatively small changes in the shape of the impedance loci as shown by Figs. 10 and 11 which correspond to cells from which 10% and 80% of the deliverable capacity has been removed. The significant changes in the impedance are that the straight line region is at precisely 45° to the real axis and the diameter of the high frequency semicircle is progressively increased as the capacity is removed. As the HgO/Hg exchange in alkali is a reversible reaction and is in a finely divided state with an extremely high effective surface area, we can conclude that the cell impedance is dominated by the zinc electrode.

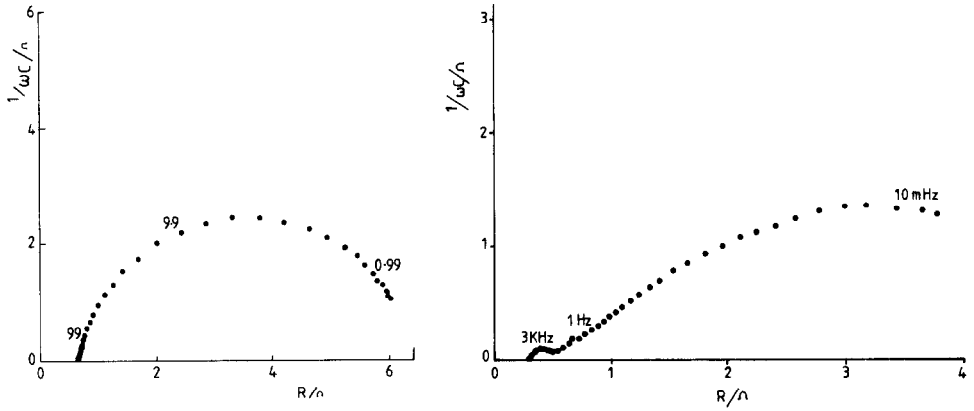

Fig. 8. As Fig. 7 but 70% of the available capacity removed.

Fig. 9. Impedance loci for a newly assembled Zn–HgO cell (Mallory type RM502R).

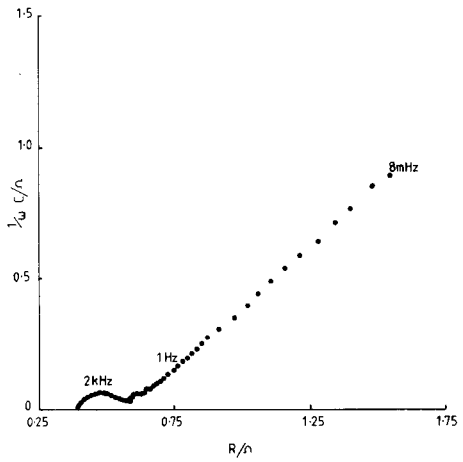

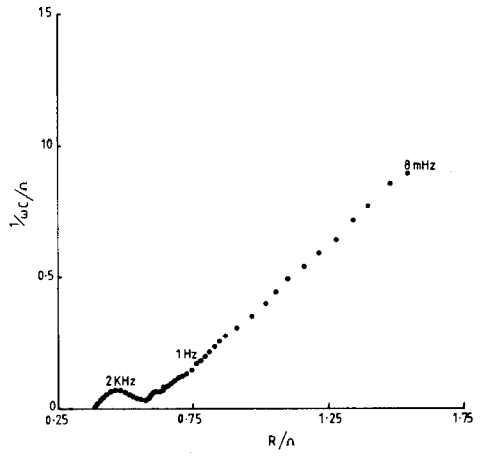

Fig. 10. Impedance loci for a cell of Fig. 9 after removal of 10% of the capacity at the 100 h rate.

Fig. 11. As Fig. 10 but 80% of the capacity removed.

We interpret the 38° Warburg slope of the newly-assembled cell to be a consequence of surface roughness; the loss of this on discharge is due to the enrichment of the remaining zinc metal surface with mercury which forms a more planar front. A further factor is probably the ZnO formed in any electrode voids, which would also tend to flatten the discharging surface. The crucial point, however, is that "porous" zinc in this cell is not porous in the electrochemical sense. This is due to the incorporation of mercury in the metal powder and also due to the particle morphology.

The return to the real axis at low frequency is due to the small electrode separation. When the time available for the electroactive species to diffuse between the electrodes approaches the same order as the period of the applied a.c., a relaxation occurs in the variation of the impedance with frequency as the concentrations of the diffusing species fall to zero at a finite distance from the electrodes [7]. The mass transport problems posed are similar to the case of a thin layer cell and, for $\Delta C = 0$ at a distance, $a/2$, halfway between the electrodes, we can calculate that:

$$Z' = \sigma_i \omega^{-1/2} \left[\frac{\sinh(U_i) + \sin(U_i)}{\cosh(U_i) + \cos(U_i)}\right] \tag{3}$$

$$Z'' = \sigma_i \omega^{-1/2} \left[\frac{\sinh(U_i) - \sin(U_i)}{\cosh(U_i) + \cos(U_i)}\right] \tag{4}$$

$$U_i = \sqrt{2a}\left(\frac{\omega}{D_i}\right)^{1/2} \tag{5}$$

$$Z'_{F\omega \to 0} = \theta + \sigma_i a \left(\frac{1}{2D_R}\right)^{1/2} + \sigma_i a \left(\frac{1}{2D_o}\right)^{1/2}. \quad (6)$$

When the separation of the electrodes is large compared with the characteristic distance ω/D, the term U_i is large and these equations become the usual Warburg impedances and the low frequency line will be at 45°. When a is small, as the frequency decreases, U_i becomes small and the imaginary component of the Warburg impedance approaches zero so that the locus returns to the real axis at very low frequency to the so-called value R_{DC} given by eqn. (6). We have been able to match the data using a simple Randles circuit for charge-transfer and diffusion but including the relaxation due to the proximity of the electrodes. This is shown in Fig. 12 and indicates that the inter-electrode distance is 0.02 cm. This distance agrees well with the manufacturers' value.

The amount of available charge in this particular system correlates very well with the charge-transfer resistance θ. This is shown in Fig. 13 in which $1/\theta$ is plotted against percentage state of charge.

A more interesting cell is the alkaline zinc–manganese dioxide cell [8]. Figure 14 shows the impedance of the newly assembled cell and Fig. 15 shows a similar cell after 12 months' storage. Here again, the simple high frequency semicircle and Warburg line are observed and this pattern is unaffected by discharging at least 10%, as shown in Fig. 16. After about 20% of the rated capacity has been removed, however, the impedance loci is materially affected (Fig. 17). The semicircle becomes elongated along the real axis and this is continued until we can clearly pick out 3 arcs at the 50% discharged level, as shown in Fig. 18. The interpretation of these data follows when the slowness of the MnO_2 reduction reaction is

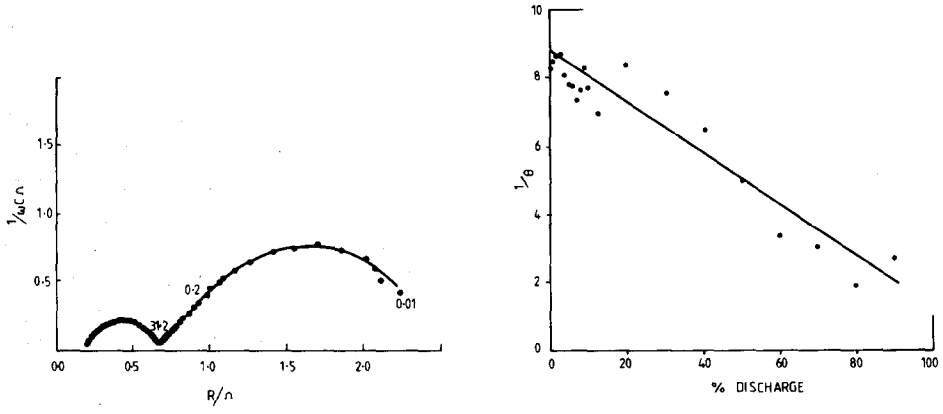

Fig. 12. Match of Zn–HgO system to a Randles circuit excluding correction for an electrode separation of 0.02 cm.

Fig. 13. The relationship between θ and state-of-charge.

considered. This results in the need to include the kinetics of the manganese dioxide reduction as part of the current-controlling mechanism. This involves considering the processes:

$$MnO_2 + H_2O + e \rightarrow MnOOH + OH^- \quad (7)$$

$$MnOOH + H_2O + e \rightarrow Mn(OH)_2 + OH^-. \quad (8)$$

Reaction (8) occurs, to a large extent, only in the latter parts of the discharge and is more complex than is shown in the equation, being as follows:

$$MnOOH + H_2O \rightarrow Mn^{3+} + 3OH^- \quad (9)$$

$$Mn^{3+} + e \rightarrow Mn^{2+} \quad (10)$$

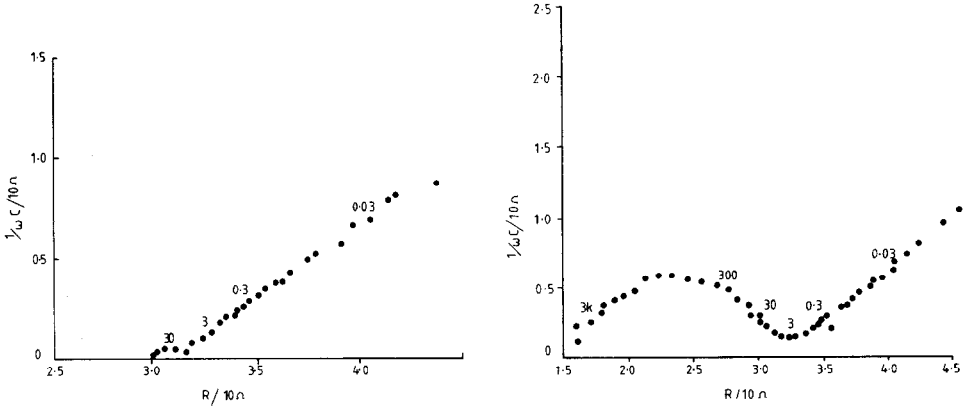

Fig. 14. The impedance loci of a newly-assembled alkaline Zn–MnO_2 cell (Mallory type MN 1500).

Fig. 15. As. Fig. 14 but after 12 months storage.

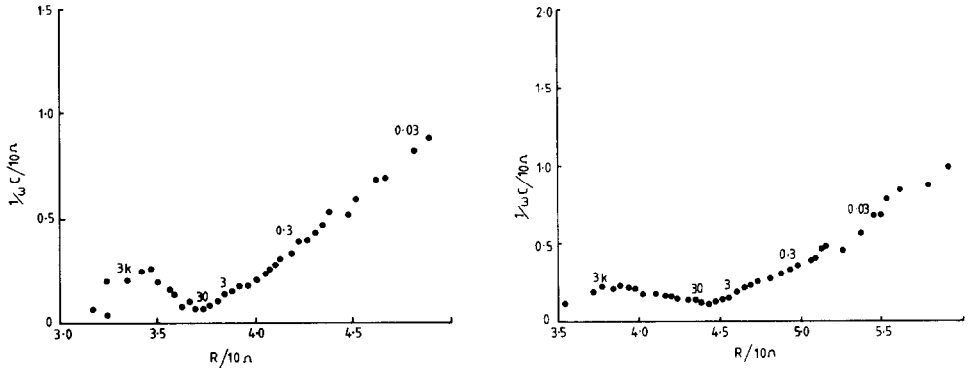

Fig. 16. Impedance loci corresponding to the cell of Fig. 14 but discharged 10% at the 100 h rate.

Fig. 17. As Fig. 16 but discharged 20%.

$$Mn^{2+} + 2OH^- \rightarrow Mn(OH)_2. \quad (11)$$

The electrode analogue corresponding to these reactions is shown in Fig. 19. The additional electrical components account for chemical reactions (9) and (11). The experimental data were matched to this model using a Taylor theorem expansion together with a least squares technique to reduce the equations for the "n" data points to the requisite number in order to solve the linear equations by a matrix inversion process.

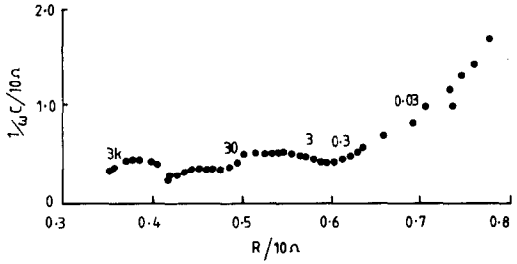

Fig. 18. As Fig. 16 but discharged 50%.

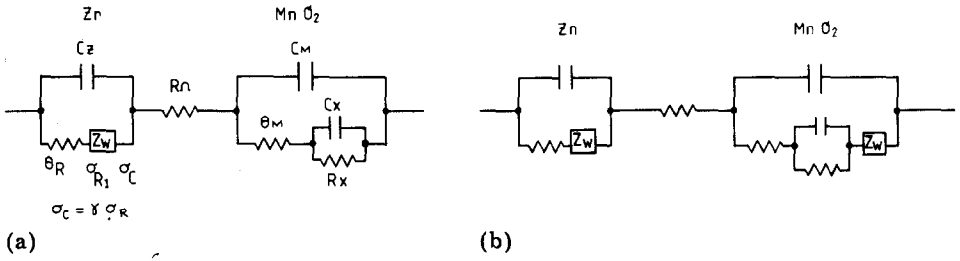

Fig. 19. Electrode analogue for the reaction sequences (a) eqns. (7) and (8), (b) eqns. (9) - (11).

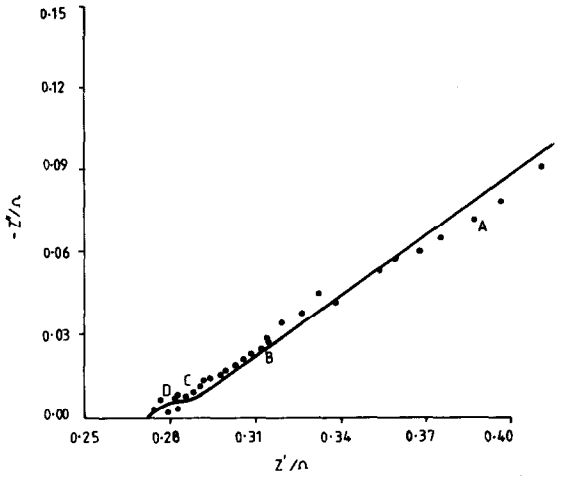

Fig. 20. Computer match of the data of Fig. 14 using a Randles circuit.

For discharge at the 10% level, the simple Randles circuit is satisfactory (Fig. 20). At 20% the additional electrode impedance has to be included. Figure 21 shows the computer match using the optimised values for the 20% case; the agreement is excellent. We have been unable to find a Warburg component for the MnO_2 electrode, however, and this indicates that the electrode must have a very large surface area so that the Warburg coefficient, σ, is very small. It was found that this cell could generally be matched by omitting the Warburg from the MnO_2 electrode and introducing a γ factor ($=\sigma_C/\sigma_R$) to account for a certain surface roughness. Figure 22 shows the results for the 50% discharged cell and Fig. 23 shows similar data for the 70% discharged cell. The matches are excellent and indicate that within the limits of experimental scatter the cells behave

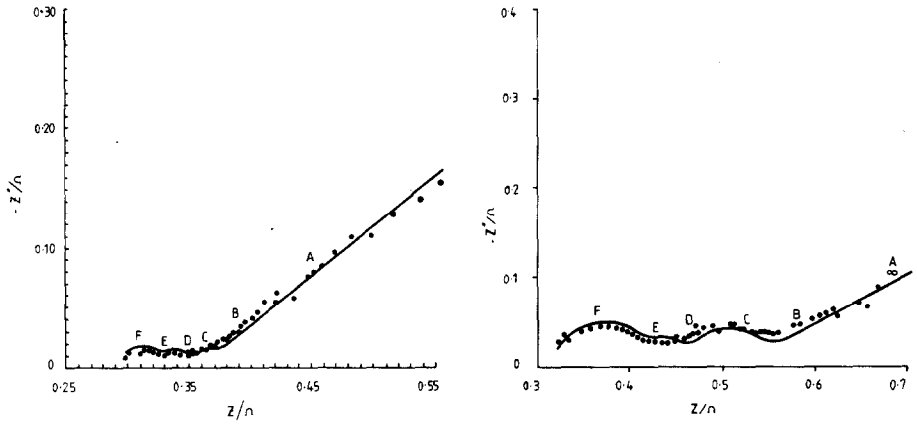

Fig. 21. Computer match of the data of Fig. 17 using the circuit of Fig. 19.

Fig. 22. As Fig. 21 but for the 50% discharged condition.

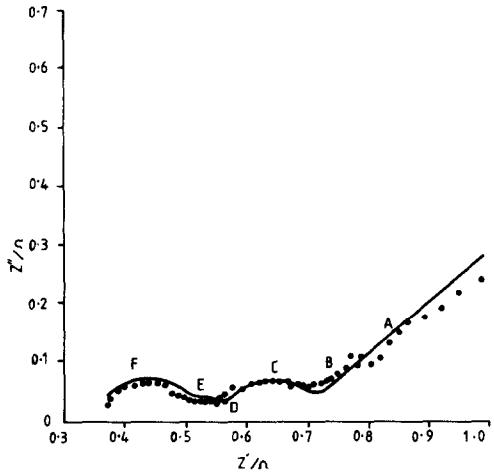

Fig. 23. As Fig. 21 but for the 70% discharged condition.

TABLE 2

Salient data for typical alkaline Zn–MnO_2 cells. Type MN1500

Discharge (%)	O.C.V. (V)	R_e (Ω)	θ_z (Ω)	C_z (F)	σ ($\Omega\ s^{-1/2}$)	γ	θ_M (Ω)	C_M (F)	R_X (Ω)	C_X (F)
0	1.573	0.274	0.0071	0.21	0.047	0.74	—	—	—	—
5	1.501	0.299	0.0189	0.051	0.039	0.78	—	—	—	—
10	1.466	0.389	0.0201	0.078	0.039	0.80	—	—	—	—
20	1.418	0.295	0.0315	0.001 95	0.039	0.85	0.0216	0.0409	0.014	2.467
30	1.374	0.310	0.0405	0.001 30	0.064	0.7	0.0369	0.0310	0.024	0.6417
50	1.324	0.32	0.0928	691×10^{-6}	0.071	0.6	0.0498	0.0196	0.0623	0.350
60	1.287	0.349	0.1198	663×10^{-6}	0.0478	1.0	0.0197	0.0197	0.0987	0.307
70	1.246	0.360	0.1464	461×10^{-6}	0.0696	0.9	0.0598	0.0190	0.1109	0.335
80	1.188	0.4	0.1964	370×10^{-6}	0.156	0.3	0.203	0.0135	—	—

as combinations of electrodes in the expected manner. Table 2 shows the kinetic data calculated from the mathematical matching process. For the MnO_2 electrode the double layer capacitance (and the area) are always considerably in excess of those of the zinc electrode. The increase in the "electrolyte" resistance of the cell reflects the build-up of ZnO in the electrode.

It is interesting that porous Zn characteristics are not obscured with the powdered Zn electrodes. This is an important point for it indicates that the incorporation of Hg effectively eliminates the electrode fine structure and the system becomes effectively planar.

Acknowledgements

We thank B.E.R.E.C. Group and Mallory Co. for the provision of certain materials. We thank Procurement Executive, Ministry of Defence, for financial support to S.A.G.R.K.

List of symbols

R	Equivalent cell resistance
C	Equivalent cell capacitance
ω	Angular frequency of the a.c. ($=2\pi f$)
Z', Z''	Real and imaginary components of the cell impedance
W	Warburg impedance
σ_R, σ_C	Warburg coefficients of the resistive and capacitative components
γ	Porosity factor ($=\sigma_C/\sigma_R$)
θ	Charge transfer resistance
C_L	Capacitance of the double layer
R_Ω	Ohmic resistance
ΔC	a.c. component of the concentration of the diffusing species
a	Electrode separation
D_R, D_o	Diffusion coefficients of the reduced and the oxidised species

References

1 J. E. B. Randles, *Discuss. Faraday Soc., 1* (1947) 11.
2 B. Ershler, *Discuss. Faraday Soc., 1* (1947) 269.
3 See, *e.g.*, J. P. G. Farr and N. A. Hampson, *Trans. Faraday Soc., 62* (1966) 3, 502.
4 N. A. Hampson and M. J. Willars, *Surf. Technol., 7* (1978) 247.
5 J. H. Sluyters, *Rev. Trav. Chim., 79* (1960) 1092.
6 S. A. G. R. Karunathilaka, N. A. Hampson and R. Leek, *Surf. Technol., 13* (1981) 339.
7 S. A. G. R. Karunathilaka, N. A. Hampson, T. P. Haas, R. Leek and T. J. Sinclair, *J. Appl. Electrochem., 11* (1981) 573.
8 S. A. G. R. Karunathilaka, N. A. Hampson, R. Leek and T. J. Sinclair, *J. Appl. Electrochem., 11* (1981) 365.